Polarization and Substructures in Protoplanetary Disks

None Assigned

ABSTRACT

We have completed a high-angular-resolution survey of 20 protoplanetary disks using data from an ALMA Cycle 4 Large Program. We find a multitude of small-scale substructure, the most common of which are rings, gaps, and spirals. Here we propose to search for polarized emission in three targets whose substructure is representative of the most common features seen in the Large Program results. Such small-scale features are thought to affect the polarization of dust continuum emission, where the polarization fraction can vary by more than an order of magnitude in, e.g., bright rings vs. depleted gaps. The main goal of our proposed observations is to search for these predicted variations in polarization in the substructures present in our targeted disks.

PI NAME:	Laura Perez			**SCIENCE CATEGORY:**	Circumstellar disks, exoplanets and the solar system
ESTIMATED 12M TIME:	**12.0 h**	**ESTIMATED ACA TIME:**	**0.0 h**	**ESTIMATED NON-STANDARD MODE TIME (12-M):**	**12.0 h**
CO-PI NAME(S): (Large & VLBI Proposals only)					
CO-INVESTIGATOR NAME(S):	Charles Hull; Zhaohuan Zhu; Xuening Bai; Myriam Benisty; John Carpenter; Sean Andrews; Jane Huang; David Wilner; Nicolás Kurtovic; Cornelis Dullemond				
DUPLICATE OBSERVATION JUSTIFICATION:					

REPRESENTATIVE SCIENCE GOALS (UP TO FIRST 30)

SCIENCE GOAL	POSITION	BAND	ANG.RES.(")	LAS.(")	ACA?	NON-STANDARD MODE
AS209	ICRS 16:49:15.3035, -14:22:08.642	7	0.300	3.000	N	Y
Elias 27 and 24	ICRS 16:26:45.0250, -24:23:07.750	7	0.300	3.000	N	Y
Total # Science Goals : 2						

SCHEDULING TIME CONSTRAINTS	NONE	**TIME ESTIMATES OVERRIDDEN ?**	No

Polarization and Substructures in Protoplanetary Disks

1. Motivation

The processes of disk evolution and planet formation will leave an imprint on the distribution of solid particles at different locations in a protoplanetary disk, resulting in a variety of substructure that can be observed from optical wavelengths in scattered light (e.g., Avenhaus et al. 2018) to radio wavelengths in both dust continuum and spectral line emission (e.g., ALMA Partnership et al. 2015; Tang et al. 2017). Our recent ALMA Large Program (LP) observations (see Fig. 1 for a subset), together with several famous examples already in the literature, have provided direct evidence for the different morphologies that are present in disks.

The most common type of substructures seem to be concentric dark gaps and bright rings, which trace zones where solid particles have been depleted (dark gaps) and concentrated (bright rings). Such rings and gaps may be caused by dynamical interaction of embedded planets or companions (e.g., Bae et al. 2017), zonal flows arising from magnetic instabilities (e.g., Johansen 2009; Bai & Stone 2014), and/or may be associated with the locations of snow lines of major volatiles in the disks (e.g., Okuzumi et al. 2016). Another type of substructure that is common in scattered-light (Benisty et al. 2017), and which has also recently been seen at millimeter wavelengths (Pérez et al. 2016; Tang et al. 2017), are spiral features. Spiral-like structures may arise from density waves launched by embedded planets in the disk (e.g., Zhu et al. 2015), by large-scale gravitational instabilities (e.g., Dipierro et al. 2015), or by the presence of a perturber outside the disk (e.g., Meru et al. 2017).

Recent polarization studies at (sub)millimeter wavelengths have been powerful at revealing new physics in protoplanetary disks (see next section). Here we propose to study the effects of different substructures on the polarization morphology, by observing polarized emission in Band 7 at 0.3″ resolution for three disks that are representative of the substructures revealed in our ALMA LP: narrow rings and wide gaps (AS 209, Fig. 1a), broad rings and depleted gaps (Elias 24, Fig. 1b), and spiral arms with a narrow gap (Elias 2-27, Fig. 1c). Given that planet formation is a common process (Petigura et al. 2013), many of the variations in small-scale structure from disk to disk are likely to be signposts of planet-disk interaction. Thus, polarization studies like those we propose here will provide a new piece of the planet-formation puzzle.

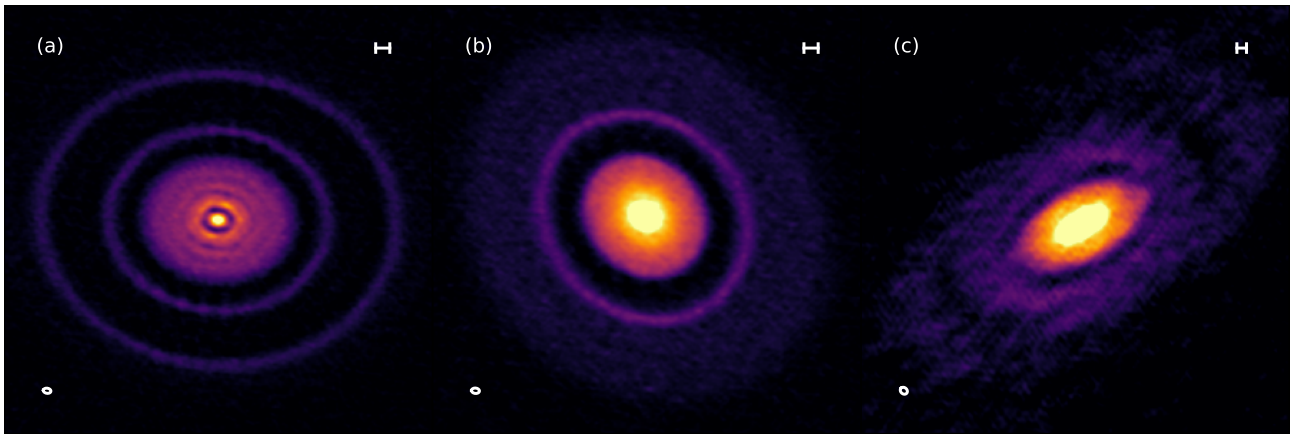

Fig. 1.— *Protoplanetary disks from our ALMA Large Program that we target in this proposal: (a) the multi-ring system in* **AS 209**, *(b) radially-wide ring substructure in* **Elias 24** *(c) spiral arms and a depleted gap in the* **Elias 2-27** *disk. Our exceptional resolution (30–50 milliarcseconds) probes down to a disk radius of* ~ 3 *au (beam size is indicated at the lower left corner); the scalebar represents* 10 *au.*

2. New physics from polarization studies

For a long time, the favored mechanism for polarizing the thermal emission from dust grains has been the presence of a magnetic field. In a protoplanetary disk, magnetic fields are necessary for driving the magneto-rotational instability (Balbus & Hawley 1991) and generating magnetized disk winds (Blandford & Payne 1982). Both these processes are thought to play a crucial role in disk evolution (e.g., Turner et al. 2014), while also creating disk substructure (e.g., Bai & Stone 2014). However, recent theoretical studies have brought forward two other mechanisms that can create polarized thermal dust emission: self-scattering of dust emission by (sub)millimeter-sized grains (Kataoka et al. 2015, 2016a; Pohl et al. 2016; Yang et al. 2016b,a) and radiative alignment of dust grains with respect to the dust emission gradient (Tazaki et al. 2017). To date, ALMA has observed polarization toward only a few disks, and while evidence for magnetically-aligned grains has been elusive, recent results are consistent with self-scattering at the shortest (Band 7) wavelengths observed (Band 7: Stephens et al. 2017; Kataoka et al. 2016b; Hull et al. 2018), or with radiative alignment at the longest (Band 3: Kataoka et al. 2017; Stephens et al. 2017).

With the exception of HL Tau, all published polarization observations are toward disks for which we do not know the underlying substructure. However, small-scale features are thought to affect the polarization fraction of dust continuum emission. For example, the simple ring-like structure analyzed by Kataoka et al. (2015), shown in Fig. 2 (left panel), results in a radial distribution of polarized sub-millimeter light that is double-peaked in the polarization fraction (Fig. 2, right panel). Here, the morphology of the polarization vectors "flip" from being oriented radially in the inner parts of the ring to being azimuthal in the outer parts of the ring (Fig. 2, right panel). Furthermore, when including dust evolution and trapping due to the presence of a planet that carves a gap, Pohl et al. (2016) find that the polarization fraction can vary by more than an order of magnitude in bright rings vs. depleted gaps.

The main goal of our proposed observations is to search for these predicted variations in polarization across the substructures pictured in Fig. 1 (i.e., narrow rings, broad rings, gaps, and spiral arms). As a secondary goal, we aim to obtain an additional constraint on dust-particle growth that is independent of the dust spectral energy distribution (SED). This is possible because submillimeter-wavelength scattering is strongly dependent on grain size, and can thus be used to estimate the maximum size of the scattering dust particles (e.g., Kataoka et al. 2016b; Stephens et al. 2017; Hull et al. 2018).

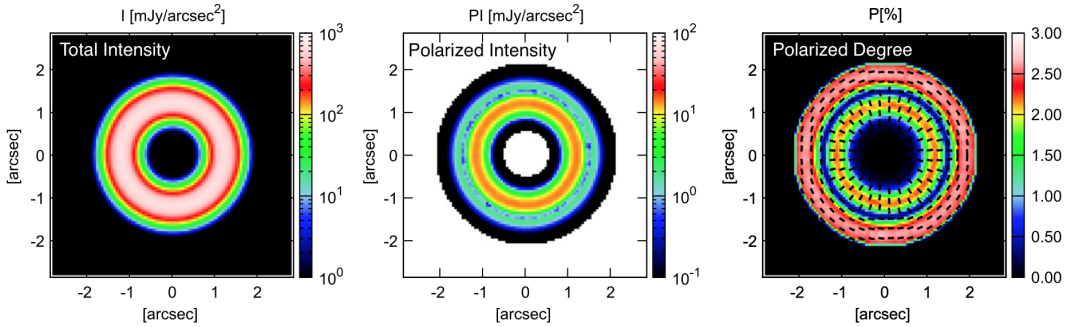

Fig. 2.— *Band 7 (870 μm) prediction for the polarization of sub-millimeter light due to self-scattering, for a protoplanetary disk with ring morphology (from Kataoka et al. 2015).* Left: *Total intensity;* center: *polarized intensity;* right: *polarization fraction in color and polarization vectors in black. A simple ring structure already has a huge impact on the polarized emission in the model; we aim to understand the impact on the polarization morphology of the substructure detected in our ALMA Large Program.*

3. Target selection and proposed observations

Based on work published over the last few years, Band 7 observations of protoplanetary disks nearly always yield polarization patterns consistent with dust scattering. Thus, it is very likely that the Band 7 polarization observations we propose here will detect polarization arising from scattering, *not* from magnetically or radiatively aligned grains. Focusing this study on Band 7, instead of longer wavelength observations in Band 6 or 3, will allow us to characterize scattering and grain growth with respect to the substructures in our three target disks. Future follow-up studies can focus on polarization at different wavelengths, in order to study, for example, the radiative alignment mechanism in Band 3 as it was done in HL Tau by Stephens et al. (2017).

Target selection: From the sample of 20 classical disks targeted in our ALMA LP, we have selected three disks that are representative of the different morphologies most commonly seen: narrow rings (AS209, Fig. 1a), wide rings (Elias 24, Fig. 1b) and spiral-like features (Elias 2-27, Fig. 1c). *Note that the substructures in these objects are already resolved at the* $\sim 0.3''$ *angular resolution that we request.* The chosen targets are those with the highest signal-to-noise ratio (SNR) at the location of the substructures, which ensures our ability to detect their polarization down to a conservative level of 1% at $> 5\sigma$.

- **AS 209** is a young ($0.5 - 1.0$ Myr; Natta et al. 2006) Class II T-Tauri star ($0.9 M_\odot$, K5 SpT, $1.5 L_\odot$; Andrews et al. 2009) located in the ρ-Oph star-forming region at a distance of 126 pc (Gaia Collaboration et al. 2016). Studies at long wavelengths constrained a radial segregation by particle size, where large particles are preferentially located closer to the star than smaller grains (Pérez et al. 2012; Tazzari et al. 2016). Recently, two concentric rings were discovered at large radii by Fedele et al. (2018), located at 75 and 130 au from the central star. Our ALMA LP observations reveal that these outermost rings are radially narrow (~ 10 au wide), while the inner disk is resolved into several more concentric rings and gaps inwards of 40 au (Fig. 1a).

- **Elias 24** is a young (~ 0.4 Myr; Andrews et al. 2010) Class II protostar that harbors one of the brightest protoplanetary disks in the ρ-Oph region ($d = 137$ pc; Ortiz-León et al. 2017), with a disk mass of $\sim 0.12\, M_\odot$ (Andrews et al. 2010). Dipierro et al. (2018) resolved some of the substructure in the disk; their hydrodynamical simulations find that the depleted gap and rings observed may arise from dynamical interactions between the disk and a single $0.7\, M_{\rm Jup}$ planet orbiting at a radius of 62 au from the central star. Our ALMA LP observations (Fig. 1b) reveal that outside of the depleted gap there is a radially broad structure of ~ 70 au in size with a bright, ~ 10 au-wide ring along its inner radius, immediately bordering the gap.

- **Elias 2-27** is young (~ 0.1 Myr; Isella et al. 2009) pre-main-sequence star in the ρ-Oph star-forming complex, and lies at a distance of 139 pc (Mamajek 2008). Classified as a Class II young stellar object, the star harbors an unusually massive ($> 0.1\, M_\odot$ Isella et al. 2009; Andrews et al. 2010) protoplanetary disk. Pérez et al. (2016) discovered substructure in the form of two symmetric spiral arms and a gap at ~ 70 au. Our ALMA LP observations reveal that the gap is quite narrow and depleted, while the spiral arms are broad, smooth features in the outer disk. **TO DO: make a better ALMA LP image of this object.**

Sensitivity estimates: The faintest of our objects in terms of substructure is Elias 2-27. Existing observations in Band 6 (1.3 mm) with an angular resolution of 0.24″ have a peak surface brightness of ~ 2 mJy/beam along the spiral arms, while the bright rings in AS209 and Elias 24 are a factor of 2 or more brighter for a similar beam size. Assuming a spectral index of $\alpha = 2.5$ and accounting for beam dilution, we expect to detect Band 7 (870 μm) continuum emission in the spiral arms at a level of 8.6 mJy/beam in the proposed 0.3″ beam. For a 1% polarization fraction, we expect to detect polarized emission in the *faintest* of the substructures at a level of 86 μJy/beam. Thus, we require a sensitivity of 17 μJy/beam to detect 1% polarization fraction above the $> 5\,\sigma$ level (i.e. a $\sim 3\sigma$ detection for a 0.5% polarization). For the brighter substructure in the three objects, our detections will be significantly stronger, even for a conservative 1% polarization fraction.

Complementary observations: Note that ^{12}CO observations were part of the LP in Cycle 4, while a successful Cycle 5 program to observe a subset of the LP disks at 3 mm is also underway (with a resubmission taking place in this Cycle to complete the sample). With these complementary gas and dust observations, we will be able to constrain the amount of trapping that large dust grains experience in these substructures, and will be able to determine whether corresponding substructures are also present in the gas. The proposed polarization observations offer us an important and unique avenue for exploring the role of substructures in the planet-formation process.

REFERENCES

ALMA Partnership, Brogan, C.L., et al., 2015. ApJ, 808:L3

Andersson, B.G., Lazarian, A., et al., 2015. ARA&A, 53:501

Andrews, S.M., Wilner, D.J., et al., 2009. ApJ, 700:1502

———, 2010. ApJ, 723:1241

Avenhaus, H., Quanz, S.P., et al., 2018. ArXiv e-prints

Bae, J., Zhu, Z., et al., 2017. ApJ, 850:201

Bai, X.N. & Stone, J.M., 2014. ApJ, 796:31

Balbus, S.A. & Hawley, J.F., 1991. ApJ, 376:214

Benisty, M., Stolker, T., et al., 2017. A&A, 597:A42

Blandford, R.D. & Payne, D.G., 1982. MNRAS, 199:883

Dipierro, G., Pinilla, P., et al., 2015. MNRAS, 451:974

Dipierro, G., Ricci, L., et al., 2018. MNRAS, 475:5296

Fedele, D., Tazzari, M., et al., 2018. A&A, 610:A24

Gaia Collaboration, Brown, A.G.A., et al., 2016. A&A, 595:A2

Hull, C.L.H., Yang, H., et al., 2018. ApJ, submitted

Isella, A., Carpenter, J.M., et al., 2009. ApJ, 701:260

Johansen, A., 2009. In K.G. Strassmeier, A.G. Kosovichev, & J.E. Beckman, eds., *IAU Symposium*, vol. 259 of *IAU Symposium*, 249–258

Kataoka, A., Muto, T., et al., 2015. ApJ, 809:78

———, 2016a. ApJ, 820:54

Kataoka, A., Tsukagoshi, T., et al., 2016b. ApJ, 831:L12

———, 2017. ApJ, 844:L5

Lazarian, A., 2007. J Quant Spec Radiat Transf, 106:225

Mamajek, E.E., 2008. Astronomische Nachrichten, 329:10

Meru, F., Juhász, A., et al., 2017. ApJ, 839:L24

Natta, A., Testi, L., et al., 2006. A&A, 452:245

Okuzumi, S., Momose, M., et al., 2016. ApJ, 821:82

Ortiz-León, G.N., Loinard, L., et al., 2017. ApJ, 834:141

Pérez, L.M., Carpenter, J.M., et al., 2012. ApJ, 760:L17

———, 2016. Science, 353:1519

Petigura, E.A., Howard, A.W., et al., 2013. Proceedings of the National Academy of Science, 110:19273

Pohl, A., Kataoka, A., et al., 2016. A&A, 593:A12

Stephens, I.W., Yang, H., et al., 2017. ApJ, 851:55

Tang, Y.W., Guilloteau, S., et al., 2017. ApJ, 840:32

Tazaki, R., Lazarian, A., et al., 2017. ApJ, 839:56

Tazzari, M., Testi, L., et al., 2016. A&A, 588:A53

Turner, N.J., Fromang, S., et al., 2014. Protostars and Planets VI, 411–432

Yang, H., Li, Z.Y., et al., 2016a. MNRAS, 460:4109

———, 2016b. MNRAS, 456:2794

Zhu, Z., Dong, R., et al., 2015. ApJ, 813:88

None Assigned

SG : 1 of 2 AS209 Band 7

Science Goal Parameters

Ang.Res.	LAS	Requested RMS	RMS Bandwidth	Rep.Freq.	Cont. RMS	Cont. Bandwidth	Poln.Prod.	Non-standard mode
0.3000"	3.0"	17.2 µJy, 1.9 mK	6414.96 km/s, 7.5 GHz	350.500000 GHz	17.199 µJy, 1.9 mK	7.500 GHz	XX,YY,XY,YX	Yes

Use of 12m Array (43 antennas)

t_total(all configs)	t_science(C43-4)	t_total()	Imaged area	#12m pointing	12m Mosaic spacing	HPBW	t_per_point	Data Vol	Avg. Data Rate
4.2 h	2.3 h	0.0 h	5.5 "	1	offset	16.6 "	8103.9 s	49.3 GB	4.0 MB/s

Use of ACA 7m Array (10 antennas) and TP Array

t_total(ACA)	t_total(7m)	t_total(TP)	Imaged area	#7m pointing	7m Mosaic spacing	HPBW	t_per_point	Data Vol	Avg. Data Rate

Spectral Setup : Single Continuum

Center Freq (Sky)	Center Freqs. SPWs	Eff #Ch p.p.	Bandwidth	Resolution	Vel. Bandwidth	Vel. Resolution	RMS
343.500000	336.500000	64	1875.00 MHz	62.500 MHz	1670.5 km/s	55.682 km/s	33.09 µJy, 4.0 mK
	338.500000	64	1875.00 MHz	62.500 MHz	1660.6 km/s	55.353 km/s	32.65 µJy, 3.9 mK
	348.500000	64	1875.00 MHz	62.500 MHz	1612.9 km/s	53.765 km/s	33.75 µJy, 3.8 mK
	350.500000	64	1875.00 MHz	62.500 MHz	1603.7 km/s	53.458 km/s	34.4 µJy, 3.8 mK

1 Target

No.	Target	Ra,Dec (ICRS)	V,def,frame --OR--z
1	1-AS 209	16:49:15, -14:22:08	-10.00 km/s,hel,RELATIVISTIC

Expected Source Properties

	Peak Flux	SNR	Linewidth	RMS (over 1/3 linewidth)	linewidth / bandwidth used for sensitivity	Pol.	Pol. SNR
Line	0.00 uJy	0.0	0 km/s			0.0%	0.0
Continuum	27.00 mJy	1569.9				1.0%	15.7

Dynamic range (cont flux/line rms): N/A

Justification for requested RMS and resulting S/N (and for spectral lines the bandwidth selected) for the sensitivity ca...

Justify 1% polarization from recent results.
pretty much every disk shows at least 1% polarization.

Justification of the chosen angular resolution and largest angular scale for the source(s) in this Science Goal.

Justification of the correlator set-up with particular reference to the number of spectral resolution elements per line ...

We are doing standard setup.

None Assigned

SG : 2 of 2 Elias 27 and 24 Band 7

Science Goal Parameters

Ang.Res.	LAS	Requested RMS	RMS Bandwidth	Rep.Freq.	Cont. RMS	Cont. Bandwidth	Poln.Prod.	Non-standard mode
0.3000"	3.0"	17.2 µJy, 1.9 mK	6414.96 km/s, 7.5 GHz	350.500000 GHz	17.177 µJy, 1.9 mK	7.500 GHz	XX,YY,XY,YX	Yes

Use of 12m Array (43 antennas)

t_total(all configs)	t_science(C43-4)	t_total()	Imaged area	#12m pointing	12m Mosaic spacing	HPBW	t_per_point	Data Vol	Avg. Data Rate
7.7 h	4.5 h	0.0 h	5.5 "	2	offset	16.6 "	8043.1 s	89.0 GB	3.9 MB/s

Use of ACA 7m Array (10 antennas) and TP Array

t_total(ACA)	t_total(7m)	t_total(TP)	Imaged area	#7m pointing	7m Mosaic spacing	HPBW	t_per_point	Data Vol	Avg. Data Rate

Spectral Setup : Single Continuum

Center Freq (Sky)	Center Freqs. SPWs	Eff #Ch p.p.	Bandwidth	Resolution	Vel. Bandwidth	Vel. Resolution	RMS
343.500000	336.500000	64	1875.00 MHz	62.500 MHz	1670.5 km/s	55.682 km/s	33.09 µJy, 4.0 mK
	338.500000	64	1875.00 MHz	62.500 MHz	1660.6 km/s	55.353 km/s	32.67 µJy, 3.9 mK
	348.500000	64	1875.00 MHz	62.500 MHz	1612.9 km/s	53.765 km/s	33.75 µJy, 3.8 mK
	350.500000	64	1875.00 MHz	62.500 MHz	1603.7 km/s	53.458 km/s	34.4 µJy, 3.8 mK

2 Targets

No.	Target	Ra,Dec (ICRS)	V,def,frame --OR-- z
1	1-Elias 2-27	16:26:45, -24:23:07	0.00 km/s,lsrk,RADIO
2	2-Elias 2-24	16:26:24, -24:16:13	0.00 km/s,lsrk,RADIO

Expected Source Properties

	Peak Flux	SNR	Linewidth	RMS (over 1/3 linewidth)	linewidth / bandwidth used for sensitivity	Pol.	Pol. SNR
Line	0.00 uJy	0.0	0 km/s			0.0%	0.0
Continuum	0.00 uJy	0.0				0.0%	0.0

Dynamic range (cont flux/line rms): N/A

Sensitivity Comments

Note that one or more of the S/N estimates are < 3. Please double-check the RMS and/or line fluxes entered and/or address the issue below.

Justification for requested RMS and resulting S/N (and for spectral lines the bandwidth selected) for the sensitivity calculation.

Justification of the chosen angular resolution and largest angular scale for the source(s) in this Science Goal.

Justification of the correlator set-up with particular reference to the number of spectral resolution elements per line width.